Lossless Data Embedding Using Generalized Statistical Quantity Histogram

Xinbo Gao, *Senior Member, IEEE,* Lingling An, Yuan Yuan, *Senior Member, IEEE,* Dacheng Tao, *Member IEEE,* and Xuelong Li, *Senior Member, IEEE*

***Abstract*—Histogram-based lossless data embedding (LDE) has been recognized as an effective and efficient way for copyright protection of multimedia. Recently, a LDE method using the statistical quantity histogram has achieved good performance, which utilizes the similarity of the arithmetic average of difference histogram (AADH) to reduce the diversity of images and ensure the stable performance of LDE. However, this method is strongly dependent on some assumptions, which limits its applications in practice. In addition, the capacities of the images with the flat AADH, e.g., texture images, are a little bit low. For this purpose, we develop a novel framework for LDE by incorporating the merits from the generalized statistical quantity histogram (GSQH) and the histogram-based embedding. Algorithmically, we design the GSQH driven LDE framework carefully so that it: 1) utilizes the similarity and sparsity of GSQH to construct an efficient embedding carrier, leading to a general and stable framework; 2) is widely adaptable for different kinds of images, due to the usage of the divide-and-conquer strategy; 3) is scalable for different capacity requirements and avoids the capacity problems caused by the flat histogram distribution; 4) is conditionally robust against JPEG compression under a suitable scale factor; and 5) is secure for copyright protection because of the safe storage and transmission of side information. Thorough experiments over three kinds of images demonstrate the effectiveness of the proposed framework.**

***Index Terms*—Generalized statistical quantity histogram, lossless data embedding, reversibility, video and image watermarking.**

Manuscript received March 31, 2010; revised July 18, 2010; accepted November 14, 2010. Date of publication March 22, 2011; date of current version August 3, 2011. This work was supported by the National Basic Research Program of China (973 Program), under Grant 2011CB707100, by the National Natural Science Foundation of China, under Grants 60771068, 60702061, 60832005, and 61072093, by the Ph.D. Programs Foundation of the Ministry of Education of China, under Grant 20090203110002, by the Natural Science Basic Research Plan in the Shaanxi Province of China, under Grant 2009JM8004, and by the Research Projector Funding of Microsoft Research Asia. This paper was recommended by Associate Editor G. Wen.

X. Gao and L. An are with the School of Electronic Engineering, Xidian University, Xi'an, Shaanxi 710071, China (e-mail: xbgao@mail.xidian.edu.cn; an.lingling@gmail.com).

Y. Yuan and X. Li are with the Center for OPTical IMagery Analysis and Learning (OPTIMAL), State Key Laboratory of Transient Optics and Photonics, Xi'an Institute of Optics and Precision Mechanics, Chinese Academy of Sciences, Xi'an 710119, Shaanxi, China (e-mail: yuany@opt.ac.cn; xuelong_li@opt.ac.cn).

D. Tao is with the Center for Quantum Computation and Intelligent Systems, Faculty of Engineering and Information Technology, University of Technology, Sydney, Broadway NSW 2007, Australia (e-mail: dacheng.tao@uts.edu.au).

Color versions of one or more of the figures in this paper are available online at http://ieeexplore.ieee.org.

Digital Object Identifier 10.1109/TCSVT.2011.2130410

I. Introduction

THE OBJECTIVE of lossless data embedding (LDE) [10], [12] is to design a embedding strategy to hide the messages into the multimedia losslessly. That is to say, the host multimedia can be recovered without any distortion after the hidden messages are extracted. The advantage has been widely demonstrated in many sensitive scenarios, e.g., medical diagnosis, remote sensing, and law enforcement.

Beginning with Barton's work [4], researchers have tried to obtain effective lossless embedding with different embedding strategies, e.g., modulo arithmetic addition [18], compression [11], difference expansion [25], and histogram [2], [3], [5]. Recently, a number of efforts [1], [19], [21] have been made for histogram-based methods and we can classify them into two categories: grayscale histogram (GH)-based and statistical quantity histogram (SQH)-based ones. Although the GH-based methods have achieved the advantages, e.g., low computational complexity and high visual quality, they fail to consider the diversity of grayscale histograms for various images. This makes their performance unstable. Moreover, the pure capacity of the GH-based methods is still a little bit low. As a consequence, our previous work [1] explored the statistical characteristics of images and shifted a SQH, i.e., arithmetic average of difference histogram (AADH), toward left and right to embed the messages. Experimental results have demonstrated that this method achieves promising performance for image quality and capacity. However, it strongly relies on the assumptions, e.g., the two peak points in AADH are regarded as -1 and 0, leading to a gap between it and real scenarios. Moreover, the capacities for texture images are a little bit lower than that for smooth images, which is caused by the flat distribution of AADH in texture images. Therefore, there is still a big room to further improve the performance of AADH-based LDE method.

In this paper, to target the aforementioned problems, to further improve the performance of SQH-based LDE, and to broaden the SQH related applications, a novel generalized SQH (GSQH) driven framework is proposed for LDE. This framework is constructed by GSQH, embedding zone selection, prevention of overflow and underflow, side information storage, and embedding and extraction procedures together. The GSQH extracts a couple of histograms as the embedding carrier, e.g., prediction error histogram (PEH) [9], difference histogram (DH) [24], AADH [1], to embed messages.

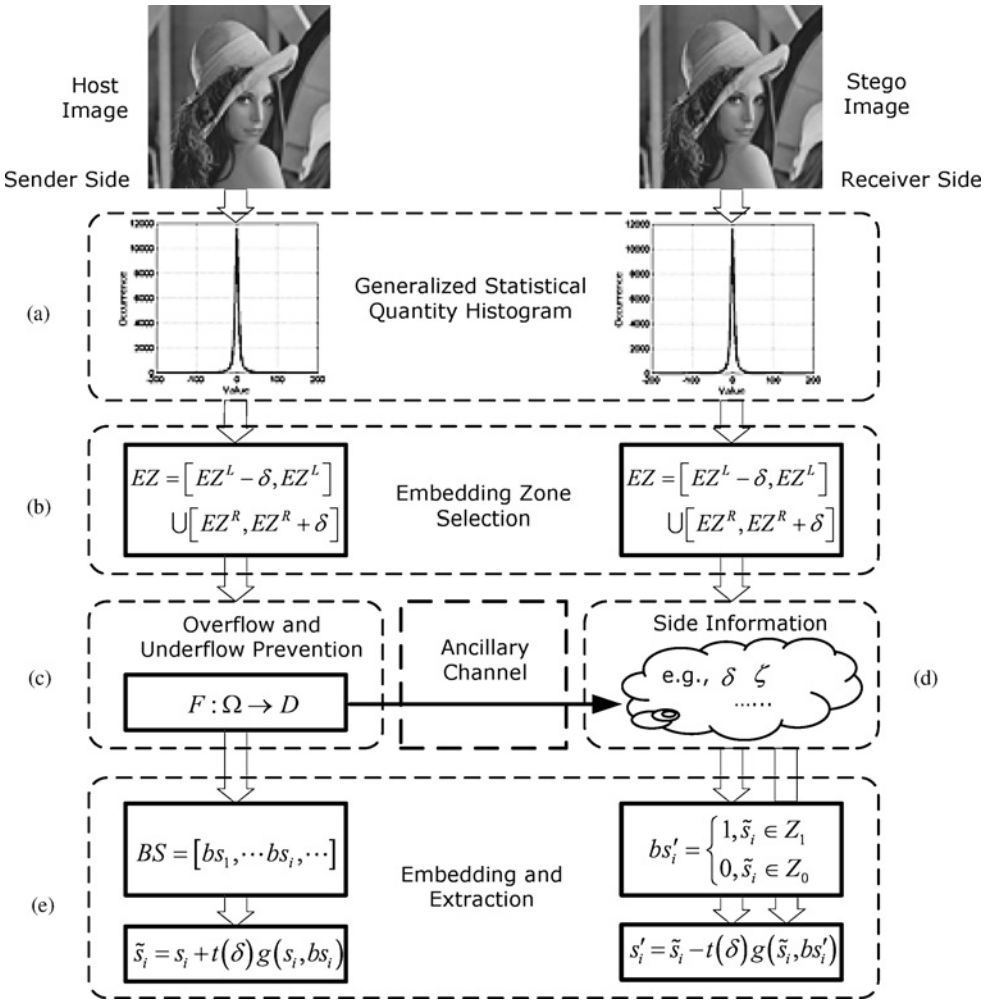

Fig. 1. LDE framework using GSQHH. (a) Construction of GSQH. (b) Embedding zone selection. (c) Prevention of overflow and underflow. (d) Side information storage. (e) Embedding and extraction procedures.

Following the embedding zone selection as well as the prevention of overflow and underflow, the lossless embedding is done. Meanwhile, to improve the security of the framework, the encryption and lossless compression techniques are utilized to store and transmit the side information efficiently and safely. Extensive experiments based on smooth images, texture images, and medical images, have been conducted to demonstrate the effectiveness of the proposed framework.

The remainder of this paper is organized as follows. In Section II, the proposed GSQH driven framework and the details of the LDE are elaborated. Experimental results and performance analysis are presented in Section III, and Section IV is our conclusion.

II. Proposed Scheme

As aforementioned, the AADH-based method [1] has two particular drawbacks: assumptions associated with SQHs of input images, low capacity especially for the images with flat AADH. In this section we describe our solutions to these drawbacks, the GSQH driven LDE framework. This framework responds to these problems by constructing the GSQH, utilizing the scale factor for embedding zone selection, designing the efficient strategies to handle the overflow and underflow of pixels as well as side information, and proposing a generalized additive spread spectrum technique to model the embedding and extraction, as shown in Fig. 1.

A. The Generalized Statistical Quantity Histogram

For histogram-based LDE methods, the distribution of histogram has an important influence on the performance. In the proposed framework, a couple of histograms observing Laplacian-like distribution, including PEH, DH, and AADH, are contained in GSQH, as shown in Fig. 2. The similar distributions can reduce the diversity of various images and guarantee the stability of the LDE methods. Among these SQHs, AADH is block based, which means the capacity can be adjusted flexibly [1]. Moreover, this blocking scheme can provide possibility for achieving robustness. Therefore, we focus on AADH and introduce the generation of it in detail.

Consider a given n-bit image with size of $M \times N$, we first divided it into non-overlapping blocks denoted as

$$\Omega = \left\{ B_i, i = 1, 2, \cdots \left\lfloor \frac{M}{m_b} \right\rfloor \times \left\lfloor \frac{N}{n_b} \right\rfloor \right\} \tag{1}$$

in which $m_b \times n_b$ is the block size, n_b is even number, and i indicates the index of each block. For $B_i = \left\{ B_i^{(p)} \right\}_{p=1}^{m_b \times n_b}$, the

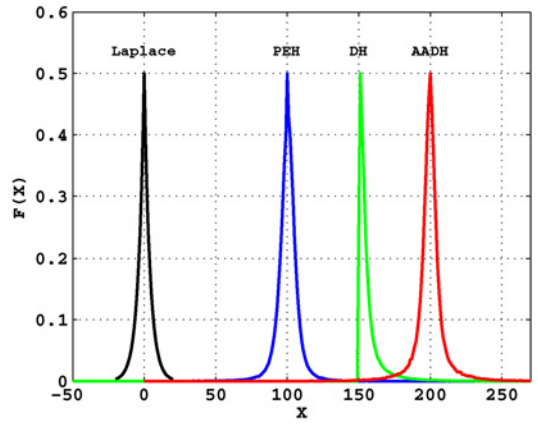

Fig. 2. Examples of Laplace distribution and GSQHs, in which the first one is the Laplace distribution with $\mu = 0$ and $\lambda = 1$ and others are the SQHs, i.e., PEH [9], DH [24], and AADH [1]. For clearness, all SQHs are normalized into the range from 0 to 0.5 and shifted toward right.

sets A and $\bar{A}$ are defined as a partition of it and $|A| = \left|\bar{A}\right| = k$. $|\cdot|$ is the cardinality of a set, i.e., the number of elements of a set. For the ith block, the arithmetic average of difference (AAD), s_i, is

$$s_i = \frac{1}{k}\sum_{j=1}^{k}\left(a_j - b_j\right) \tag{2}$$

where $\left(a_j, b_j\right)$ is called a pair, $a_j \in A$, $b_j \in \bar{A}$, and $1 \le j \le k$. In order to obtain a high capacity, s_i is expected to be very close to zero according to [20]. Therefore, an optimization problem is formulated as

$$A^* = \arg\max_{A} P\left(abs\left(s_i\right) < \varepsilon \,|\, A\right) \tag{3}$$

where ε is any positive integer. Then, how to find a suitable A is a key issue to solve this optimization problem. Inspired by the work in [20], we choose A with

$$A = \left\{ B_i^{(j)} \;\middle|\; \begin{array}{c} j = \frac{1}{2}\left[1 + \cos\left(\pi r\right)\cos\left(\pi c\right)\right]\left[\left(r-1\right)\cdot n_b + c\right] \\ j > 0 \end{array} \right\} \tag{4}$$

in which (r, c) denotes the location of an arbitrary element in B_i and $1 \le r \le m_b$ and $1 \le c \le n_b$. Based on this, the AADH of an image can be generated by applying (2) to all blocks, which will act as the embedding carrier in the next subsection. For convenience, h_x and $num(h_x)$ denote the horizontal and vertical coordinates of the xth value in AADH, respectively, and H is the set of h_x.

B. Embedding Zone Selection

For a given GSQH, e.g., AADH, the embedding zone selection determines where the messages will be embedded. In this framework, the embedding zone EZ is defined as

$$EZ = \left[EZ^L - \delta, EZ^L\right] \bigcup \left[EZ^R, EZ^R + \delta\right] \tag{5}$$

where $\delta \ge 0$ is a scale factor

$$EZ^R = \arg\max_{h_x \epsilon H} num\left(h_x\right) \tag{6}$$

and

$$EZ^L = \arg\max_{h_x \epsilon H, h_x \neq EZ^R} num\left(h_x\right). \tag{7}$$

Without loss of generality, we suppose $EZ^L \le EZ^R$. In this case, the capacity is equal to

$$\sum_{\kappa=0}^{\delta}\left(num\left(EZ^L - \kappa\right) + num\left(EZ^R + \kappa\right)\right). \tag{8}$$

From (8), it can be seen the capacity is influenced by three factors: δ, EZ^L, and EZ^R. Given EZ^L and EZ^R, we can flexibly adjust the capacity by setting suitable δ. Note that the definition of EZ in [1] can be regarded as a special case of (5) when $\delta = 0$, $EZ^L = -1$ and $EZ^R = 0$.

C. Prevention of Overflow and Underflow

In LDE, how to prevent overflow and underflow of pixels is essential. In this paper, a novel divide-and-conquer strategy is proposed to solve this problem. First, we classify the image blocks into three types via a discriminative function $F : \Omega \to D$, in which $D = \left\{R_g, S_g, U\right\}$ denotes the three types of blocks: regular, singular, and unavailable. Given a block with $s_i \ge EZ^R$ and the scale factor δ, the discriminative function is defined as

$$F = \begin{cases} R_g, & \text{if } \left(a_j < T\right) \\ S_g, & \text{if } \left(a_j \ge T\right) \text{and } \left(b_j > \delta\right) \\ U, & \text{if } \left(a_j \ge T\right) \text{and } \left(b_j \le \delta\right) \end{cases} \tag{9}$$

in which $T = 2^n - \delta - 1$. Thereafter, different strategies are adopted to modify s_i according to (2). For regular blocks, $a_j \leftarrow a_j + \delta$; and $b_j \leftarrow b_j - \delta$ for singular blocks. When a block is unavailable, it will be discarded and s_i keeps intact. Because the AADH is symmetric, F is easily extended to the case when $s_i \le EZ^L$. With the strategy, the proposed framework can be applied to various images. In order to recover the host image, the locations of singular and unavailable blocks are necessary in the receiver side. How to store and transmit side information to the receiver side is another key problem in LDE, which will be discussed in the next subsection.

D. Side Information Storage

As known, the side information is important for the receiver side to extract the hidden messages, so it is valuable to store and transmit side information efficiently and safely. In our framework, both the encryption and lossless compression techniques are adopted to solve this problem. On one hand, the location information of unavailable blocks, and several parameters, e.g., the scale factor and block size, are encrypted and transmitted to the receiver side via the ancillary channel. They served as a cryptographic key in the extraction process of the hidden messages. On the other hand, the location information of singular blocks is embedded into the host image as well as watermarks. To be specific, a flag matrix M_f, which indicates where the singular blocks are, is first compressed with a lossless compression algorithm, e.g., run-length encoding (RLE). Following this, the compressed matrix M_c is concatenated with watermarks to form the final binary message stream BS, which will be embedded into the host image in the next subsection.

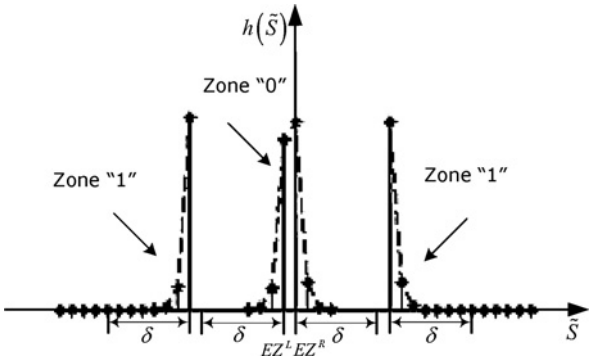

Fig. 3. Example of the stego AADH.

E. Embedding and Extraction Procedures

Consider a given block with AAD s_i and a message bit bs_i, we define the embedding rule as a generalized additive spread spectrum technique in this framework, denoted by

$$\tilde{s}_i = s_i + t(\delta)\, g(s_i, bs_i) \tag{10}$$

in which the weight function $t(\delta)$ determines the embedding strength, and the feature function $g(s_i, bs_i)$ indicates the changes of s_i in different cases. These two functions are defined as

$$t(\delta) = \delta + 1 \tag{11}$$

and

$$g(s_i, bs_i) = \begin{cases} -1, & s_i < EZ^L - \delta \\ -bs_i, & EZ^L - \delta \le s_i \le EZ^L \\ 0, & EZ^L < s_i < EZ^R \\ bs_i, & EZ^R \le s_i \le EZ^R + \delta \\ 1, & s_i > EZ^R + \delta \end{cases} \tag{12}$$

respectively. Fig. 3 shows an example of the stego AADH, in which the binary bits "0" are embedded into the central part of the histogram, denoted as $Z_0 = EZ$; and bits "1" are embedded into the side parts, denoted as

$$\begin{aligned} Z_1 = &\left[EZ^L - 2\delta - 1, EZ^L - \delta - 1\right] \\ &\bigcup \left[EZ^R + \delta + 1, EZ^R + 2\delta + 1\right]. \end{aligned} \tag{13}$$

Corresponding to the embedding process, we can deduce the extraction rules as

$$s_i' = \tilde{s}_i - t(\delta)\, g\left(\tilde{s}_i, bs_i'\right) \tag{14}$$

and

$$bs_i' = \begin{cases} 1, \tilde{s}_i \in Z_1 \\ 0, \tilde{s}_i \in Z_0 \end{cases} \tag{15}$$

in which s_i' represents the AAD of the recovered block and bs_i' means the extracted message bit. Because the embedding and extraction rules are reversible, both the host images and the hidden messages can be recovered losslessly when the stego images are not attacked.

III. Experimental Results

In this section, we evaluate the performance of the proposed framework based on the following experiments: the capacity experiment, invisibility experiment, robustness experiment, and comparison experiment, which are conducted on 300 test images, including smooth images, texture images, and medical images. At the beginning of this section, we first brief the image databases for evaluation.

The CVG-UGR image database [28] has been recognized as an important standard database for measuring the performance of data hiding methods, from which we select 100 images to constitute the smooth images. Also, we pick up 100 texture images from Brodatz textures database [29], which has been widely used by many popular databases, e.g., USC-SIPI image database. As for 100 medical images, we choose 30 MR and MRI images from DICOM sample image sets [30], 35 CT and 35 PET CT images from OsiriX website [31], respectively. To facilitate experimental comparison, all test images have a fixed size of $512 \times 512 \times 8$.

A. Capacity Experiment

In the proposed framework, the capacity is mainly influenced by the two factors: the block size and the scale factor. Given the block size, the larger the scale factor is, the more the capacity is. Given the scale factor, the smaller the block size is, the more the capacity is. Taking the image *D*2 as an example, we first make a qualitative analysis of this relationship, as shown in Fig. 4, herein, ξ is the block size, EZ^L and EZ^R are assumed to be equal to the origin of coordinate. According to (8), the capacity can be approximately regarded as the area of the region formed by the AADH envelope and δ, shown as the shadow region. On one hand, suppose $\xi = \xi_2$, with the increase of δ, i.e., $\delta_1 \to \delta_2$, the area becomes larger, namely, the capacity is increased. On the other hand, suppose $\delta = \delta_1$, the capacity is also increased with the decrease of ξ from ξ_1 to ξ_2. To further show this relationship, we conducted capacity experiment over 300 test images. The partial experimental results are presented in Fig. 5 and Table I. Fig. 5 shows the trend of capacity with the changes of ξ and δ for the image *Lena*. As shown, the capacity is increased sharply with δ when the block is small. For the bigger blocks, the increase becomes slow. Correspondingly, the influence of the block size on the capacity is more significant for the large scale factors than for the small ones. Table I shows the pure capacities for three kinds of images at different block sizes from 2×2 to 6×6 (by column), and different scale factors from 0 to 4 (by row).

To further illustrate how the block size and scale factor influence the pure capacity, we investigate the effects from two aspects in the following parts.

1) *Effects of the Block Size ξ on Pure Capacity:* Given the scale factor δ. the pure capacity is denoted as

$$PC = \left(\left\lfloor \frac{\Re}{\xi} \right\rfloor - N_U\right) \cdot \Theta \tag{16}$$

where $\Re$ is the image size, $\lfloor \cdot \rfloor$ means rounding down, N_U is the number of unavailable blocks, and Θ is a value roughly representing the range of EZ determined by δ. In practical scenario, statistical experimental results show N_U is always

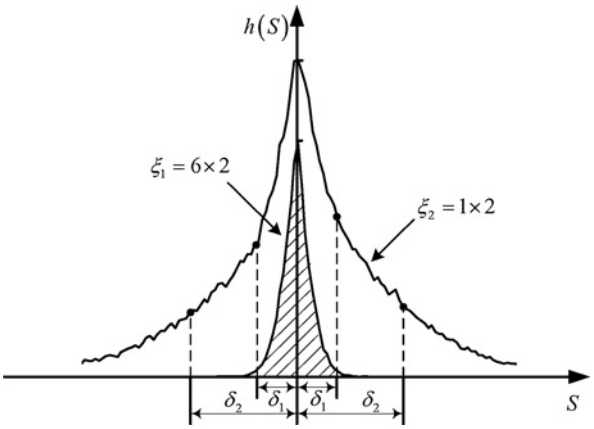

Fig. 4. Qualitative analysis of the effects of the scale factor and block size on capacity.

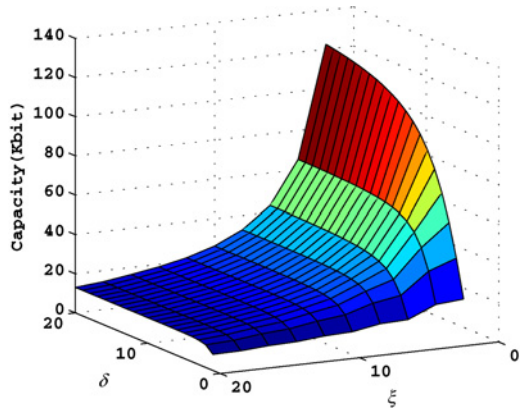

Fig. 5. Trend of capacity with the changes of the block size ξ and scale factor δ for *Lena*.

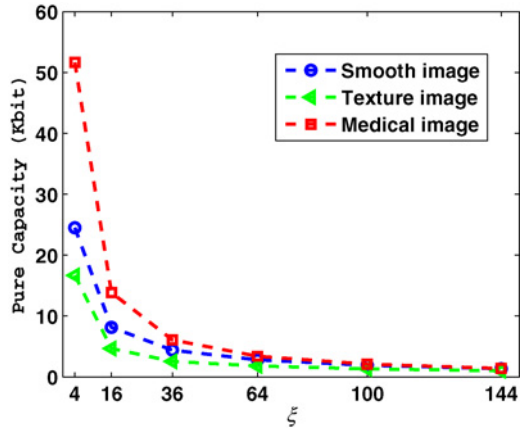

Fig. 6. Effects of the block size ξ on the pure capacity over 300 test images.

small, so the pure capacity depends on the block size ξ mainly. The larger ξ is, the lower the pure capacity is; and vice versa. Fig. 6 shows the statistical average of the pure capacities for block size ξ from 2×2 to 12×12 with step 2, herein, the scale factor δ is 0. Also observe that the pure capacity of the medical images is the highest at the same block size.

2) *Effects of the Scale Factor δ on Pure Capacity:* In this part, we will examine the effects of the scale factor δ on pure capacity. As discussed in Section II, the flag matrix together with watermarks is embedded into the host image. So the pure capacity is determined by the two parts: the capacity, C, and the compressed flag matrix, M_c, denoted as

$$PC = C - O_{M_c} = \sum_{k=0}^{\delta} \left(num(EZ^L - \kappa) + num\left(EZ^R + \kappa\right)\right) - O_{M_c} \quad (17)$$

where O_{M_c} is the size of M_c. Apart from C, M_c is also influenced by the scale factor δ. To explore the effects of δ on them, Fig. 7 compares the sizes of C and M_c for different kinds of images when the block size is set to be 1×2. In this experiment, we conduct 3000 statistical experiments over the aforementioned databases, and the scale factor δ changes from 0 to 9 with step 1. The statistical average shows the sizes of C and M_c increase with the increase of δ, and the change of C is more significant than that of M_c. This is the reason why the pure capacity can be improved by increasing δ. Based on this, Fig. 8 shows statistical average of the changes of the pure capacity with the increase of δ from 0 to 9 for three kinds of images, which further demonstrates the effectiveness of δ on improving the pure capacity. An exception is when $\delta > 4$ is applied to medical images. In this case, the pure capacity gets decreasing because the increment of M_c is larger than that of C.

B. Invisibility Experiment

In this subsection, invisibility experiments are conducted to evaluate the distortion of the stego images versus the host ones. It is universally agreed that the peak signal-to-noise ratio (PSNR) is used as an evaluation criteria by

$$PSNR = 10 \log \left(\frac{255^2}{MSE}\right) \quad (18)$$

where MSE is the mean squared error between the stego image and the host one. Based on (10), it can be seen that two factors influence MSE: the scale factor and changed AADs. Suppose the size of the host image is $\Re$, and the number of the changed AADs is λ, MSE can be obtained by

$$MSE = \frac{1}{\Re} \cdot \frac{\lambda \cdot \xi}{2} \cdot t^2(\delta) \quad (19)$$

and

$$\lambda = \sum_{\kappa \geq \delta + 1} num\left(EZ^L - \kappa\right) + num\left(EZ^R + \kappa\right) + \gamma \quad (20)$$

where γ means the number of the bit "1" in the binary message stream. With (19), the PSNR can be represented by

$$PSNR = 10 \log \left(\frac{255^2 \cdot 2 \cdot \Re}{\lambda \cdot \xi \cdot t^2(\delta)}\right). \quad (21)$$

In the worse case, all AADs will be changed, namely, $\Re = \lambda \cdot \xi$, the lower bound of PSNR is

$$PSNR = 10 \log \left(\frac{255^2 \cdot 2}{t^2(\delta)}\right). \quad (22)$$

TABLE I
PURE CAPACITIES FOR SMOOTH IMAGES, TEXTURE IMAGES, AND MEDICAL IMAGES

Image	δ	Pure Capacity (bit)			Image	δ	Pure Capacity (bit)			Image	δ	Pure Capacity (bit)		
		2×2	4×4	6×6			2×2	4×4	6×6			2×2	4×4	6×6
Lena	0	20 762	9350	5425	D1	0	18 096	9714	5736	M1	0	52 196	15 593	7137
	1	36 275	13 734	6814		1	33 466	13 977	6978		1	59 991	16 157	7198
	2	46 715	15 247	7121		2	44 243	15 455	7159		2	62 542	16 311	7199
	3	53 176	15 820	7194		3	51 858	15 920	7193		3	63 723	16 354	7199
	4	57 142	16 084	7208		4	56 661	16 110	7198		4	64 358	16 365	7199
Boat	0	20 162	9635	5894	D25	0	31 610	11 917	5814	M2	0	50 459	15 041	7045
	1	36 109	13 729	6924		1	45 129	14 192	6786		1	56 963	15 924	7189
	2	46 446	15 178	7145		2	51 162	15 126	7063		2	59 922	16 210	7198
	3	52 519	15 762	7201		3	53 969	15 628	7144		3	61 651	16 307	7199
	4	56 210	16 067	7210		4	55 974	15 916	7165		4	62 810	16 340	7199
Sailboat	0	11 556	5123	3890	D30	0	24 917	11 295	5981	M3	0	52 488	15 699	7137
	1	21 473	8967	5904		1	41 580	14 520	6851		1	59 946	16 205	7204
	2	29 889	11 751	6785		2	51 159	15 443	7048		2	62 537	16 317	7210
	3	36 726	13 617	7065		3	56 279	15 780	7071		3	63 756	16 355	7211
	4	42 623	14 844	7156		4	59 086	15 944	7083		4	64 426	16 360	7211
Blackb	0	23 048	9883	5749	D43	0	26 943	11 131	5397	M4	0	55 826	15 921	7181
	1	40 997	14 473	7046		1	42 391	13 224	6173		1	62 325	16 279	7198
	2	52 455	15 753	7188		2	50 057	13 834	6605		2	64 054	16 323	7198
	3	58 530	16 099	7207		3	53 488	14 220	6891		3	64 747	16 344	7198
	4	61 475	16 244	7211		4	55 120	14 590	7050		4	65 088	16 351	7198
Airplane	0	30 101	12 009	6210	D59	0	28 933	12 806	6529	M5	0	50 259	15 191	7067
	1	45 722	14 641	6960		1	45 781	15 325	7118		1	57 637	15 977	7184
	2	53 232	15 548	7162		2	54 555	15 981	7177		2	60 853	16 195	7197
	3	57 281	15 975	7207		3	59 011	16 184	7190		3	62 522	16 278	7198
	4	59 483	16 173	7211		4	61 199	16 233	7165		4	63 548	16 318	7199
Crowd	0	30 319	10 580	5564	D70	0	28 363	2915	1525	M6	0	49 061	15 227	7037
	1	42 393	13 341	6554		1	28 482	4685	2735		1	57 813	16 017	7194
	2	48 685	14 604	6773		2	29 986	6458	3632		2	61 043	16 216	7207
	3	52 479	15 169	6789		3	30 077	8138	4421		3	62 678	16 303	7210
	4	55 322	15 403	6789		4	39 522	9183	4974		4	63 541	16 331	7211

By contrast, when all the bits of the binary message stream are "0," the upper bound of PSNR is

$$PSNR = 10\log\left(\frac{255^2\cdot 2\cdot \Re}{\lambda^*\cdot\xi\cdot t^2(\delta)}\right) \tag{23}$$

where

$$\lambda^* = \sum_{\kappa\geq\delta+1} num\left(EZ^L-\kappa\right)+num\left(EZ^R+\kappa\right). \tag{24}$$

Fig. 9 shows the examples of stego images and the host ones at different δ. It can be seen that PSNR is decreased with the increase of δ. More importantly, the stego images can hardly be distinguished from the host ones.

C. Robustness Experiment

In the AADH-based LDE method [1], the hidden messages are only conveyed through lossless environment. This means a slight change of the stego images can make the correct recovery of the messages impossible. For some applications, however, it is desired that the LDE methods are robust against some unmalicious image processing, such as JPEG compression. An example is that the medical images are transmitted to a family doctor after lossy compression [5]. Fortunately, the proposed GSQH driven LDE framework offers such ability due to the introduction of the scale factor. To test the robustness against JPEG compression, we consider a simple scenario, similar to [5], [20]. That is, a message of 100 bits is embedded into the image repeatedly. At the receiver side, we use majority voting to decode the hidden message bits. Fig. 10 shows the statistical experimental results of robustness, in which the block size is 8×8 and the scale factor δ is from 0 to 29. By adjusting δ, our framework is robust against JPEG compression even when the JPEG quality factor is 30. Meanwhile, we also notice that the robustness cannot work at some JPEG quality factors for a given δ. Through the analysis of experimental results, we find that this is caused by different effects of JPEG compression with different factors on the AADHs. As shown in Fig. 11(b), when the quality factor is 80, all elements in AADH are all constricted to the zone "0," which is totally different from the original distribution of the embedding zones. At the receiver side, this means the hidden bits "1" will be wrongly regarded as "0" and thus leads to the failure of watermarking recovery. In future work, we will focus on this problem and improve the robustness of the proposed framework.

D. Comparison Experiment

In this subsection, some experiments are conducted on three kinds of images to compare the performance of the proposed framework with three histogram-based LDE methods, includ-

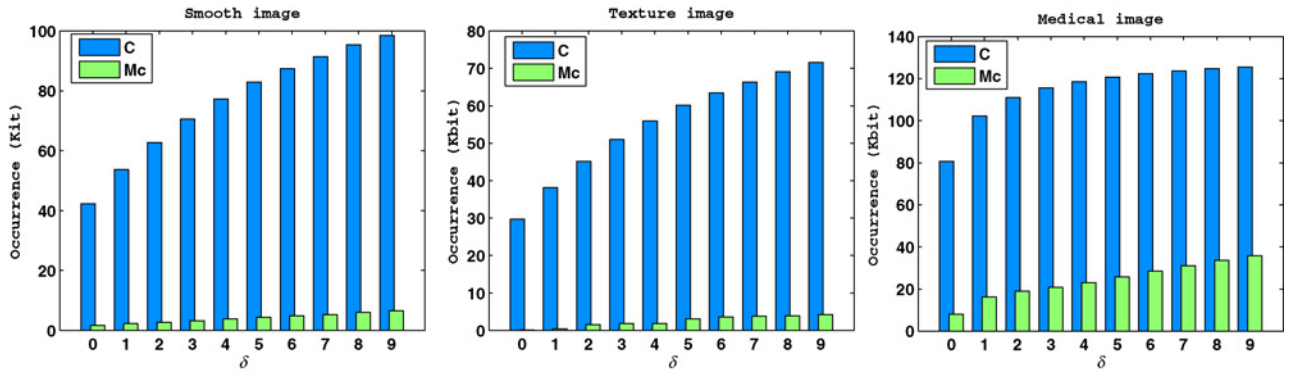

Fig. 7. Size comparison between C and M_c for different kinds of images. The x-coordinate represents the scale factor δ, y-coordinate represents the occurrences of C and M_c, which are used to evaluate the size of them.

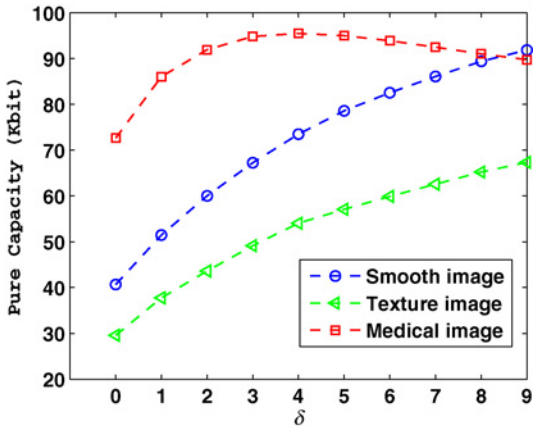

Fig. 8. Effects of the scale factor δ on the pure capacity over 300 test images.

ing two methods based on GH [19], [21] and one based on SQH [1]. First, we select some special images to demonstrate the better adaptability of the proposed framework than that of [1]. Then, we compare the aforementioned methods in terms of the pure capacity versus PSNR.

1) *Adaptability:* In the proposed LDE framework, we employ a novel divide-and-conquer strategy to solve the overflow and underflow problems, which not only removes the assumption in [1], but also broadens the applications of our framework. For various images, both the host images and the hidden messages can be recovered without distortion when the stego images are not destroyed by the attackers. Fig. 12 illustrates the recovered images when the proposed framework and the method in [1] are applied to the medical image, *M8*, in which the block size is 6×6 and the scale factor is 0. As shown, some blocks marked by the yellow squares in Fig. 12(b) cannot be recovered losslessly using the method in [1]. In practical scenarios, these blocks may disturb the diagnosis of disease. By contrast, the proposed framework works well, shown in Fig. 12(c). This advantage has been further demonstrated by the extensive experiments over other images.

2) *Pure Capacity Versus Image Quality:* In this part, we compare the pure capacity in bit/pixel versus image quality in PSNR delivered by the proposed framework with three histogram-based LDE methods. For a fair comparison, we also apply these methods to the 300 test images. The statistical average is illustrated in Fig. 13, from which it can be seen that the SQH-based LDE methods, i.e., the work in [1] and the proposed GSQH driven framework, give much better performance than those in [19] and [21] based on GH in terms of the stability as well as the adaptability. To be specific, the pure capacity of Ni's method varies from different kinds of images greatly. Hwang's method fails to work for almost all the medical images because it is difficult to find out the desired symmetric peaks in the unilateral grayscale histograms of the medical images. These drawbacks are all caused by the diversity of the grayscale histograms for different images. By contrast, the similarity of SQH for different images not only reduces the diversity but also ensures better stability and adaptability. Among two SQH-based LDE methods, the GSQH driven framework has outperformed that in [1] in capacity. Given the similar PSNR, the proposed framework achieves much higher capacity. Also it is observed that the more flexible capacity control is obtained in our framework, which is helpful to make a tradeoff between the capacity and the image quality according to the different practical requirements.

E. Summary

As discussed above, extensive experiments are carried out to evaluate the performance of the proposed GSQH driven LDE framework and demonstrate that it outperforms the related histogram-based methods. Advantages of this framework are listed as follows.

1) *General purpose:* Some different SQHs, e.g., PEH, DH and AADH can be applied in the framework for LDE. All these histograms are used as the embedding carrier, whose similar statistical characteristics for different images can reduce the diversity of the grayscale histograms and achieve stable performance of the LDE methods.
2) *Better adaptability:* The novel divide-and-conquer strategy is employed to prevent overflow and underflow. With this strategy, the proposed framework can be applied to various images, which is also demonstrated by a large number of experiments. In addition, the proposed framework is robust against the JPEG compression by selecting the suitable scale factor. This means the hidden

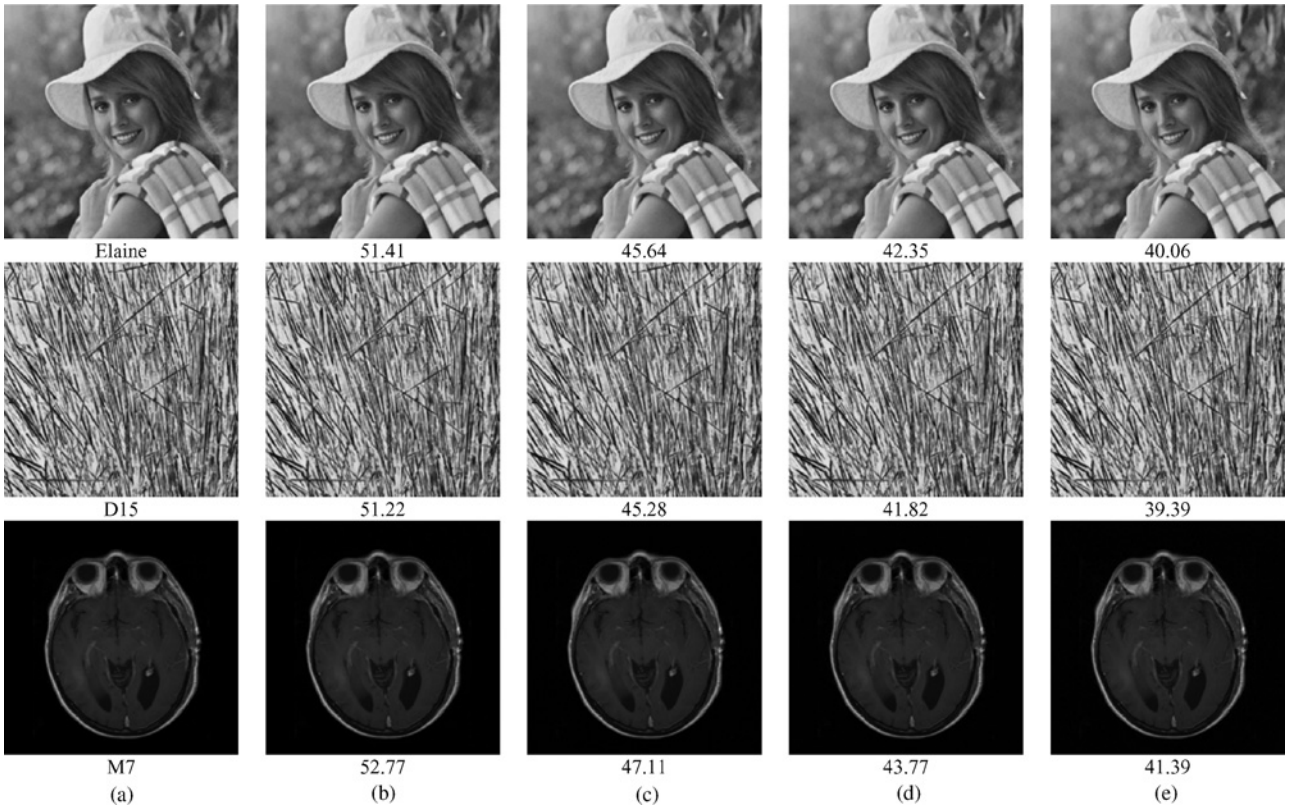

Fig. 9. Host and stego images at different δ. (a) Host images. (b)–(e) Stego images with PSNR (dB) below. (b) $\delta = 0$. (c) $\delta = 1$. (d) $\delta = 2$. (e) $\delta = 3$.

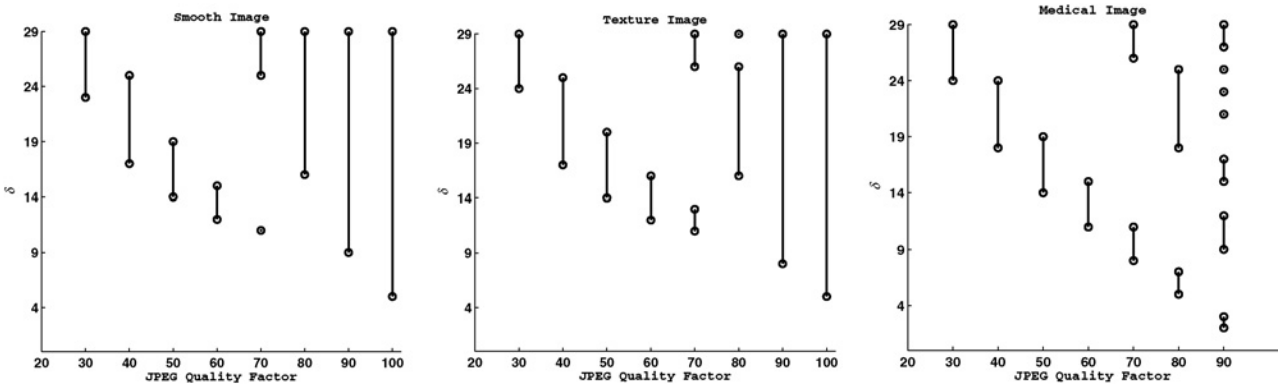

Fig. 10. Illustration of robustness against JPEG compression. For each JPEG quality factor, the line and circles represent the values of δ at which the embedded watermarks can be recovered correctly when the stego images are attacked.

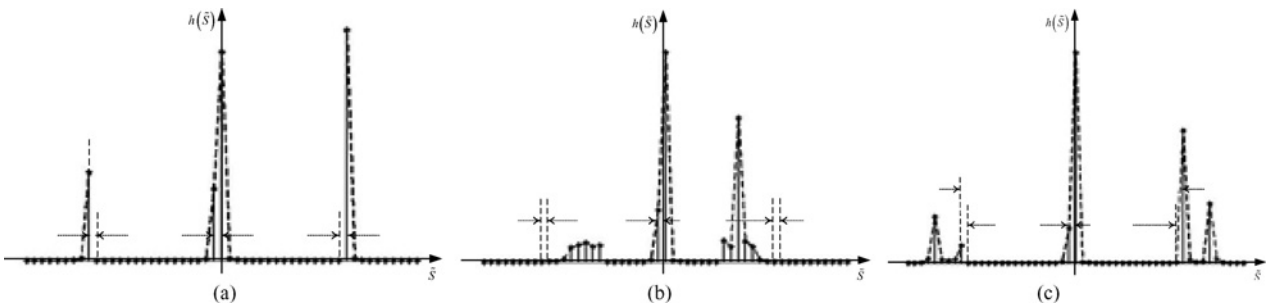

Fig. 11. Examples of AADHs in different cases. (a) Unattacked AADH. (b), (c) Attacked AADHs by JPEG compression with factors of 80 and 50, respectively.

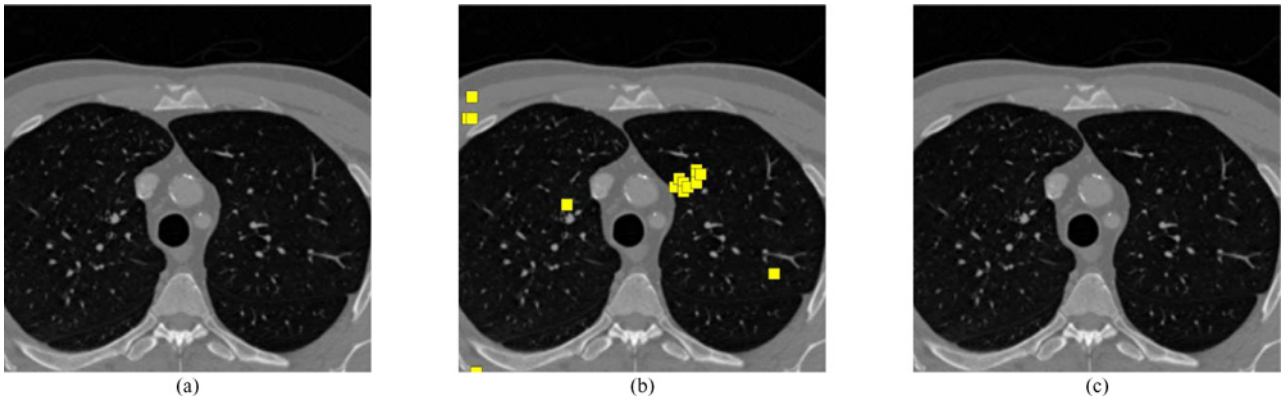

Fig. 12. Comparison of the recovered images between the proposed framework and the method in [1]. (a) Host image. (b) Recovered image using the method in [1]. (c) Recovered image using the proposed framework. The yellow squares in (b) represent the unrecovered blocks.

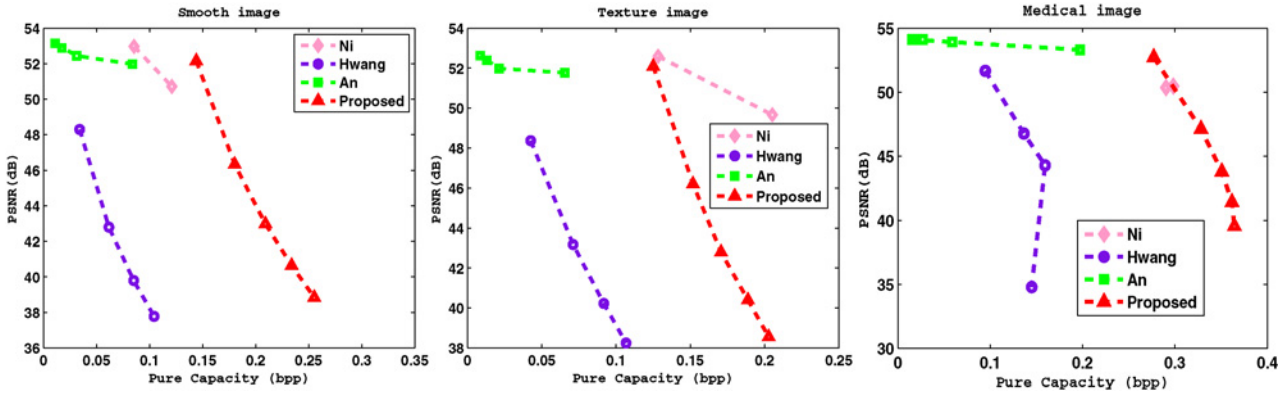

Fig. 13. Performance comparison between the proposed framework and three existing LDE methods based on histogram, i.e., Ni [21], Hwang [19], and An [1] for three kinds of images, including smooth images, texture images, and medical images.

messages can be conveyed through the lossy environment, which further improves the adaptability of our framework.

3) *Flexible capacity control:* The proposed framework contains two free parameters, the block size and the scale factor, for adjusting the capacity. When a lower capacity is needed, e.g., for content authentication purpose, we can change the block size while keeping the scale factor constant, e.g., 0, to satisfy the requirement. In this way, a higher image quality can be achieved. On the other hand, when the capacity cannot be increased by decreasing the block size, we can change the scale factor to achieve a higher capacity. Although the image quality is degraded in this case, the differences between the host image and the stego image are so little that we cannot distinguish them with our eyes. Moreover, we can use this way to improve the capacities of texture images, as shown in experiments.
4) *Higher security:* In the proposed framework, the lossless compression and encryption are adopted to handle the storage and transmission of the side information. At the receiver side, this information is essential to recover the hidden messages and the host image. In other words, the malicious attackers cannot steal the hidden secrets without it. This mechanism, therefore, is worthwhile for the copyright protection.

IV. Conclusion

In this paper, a generalized LDE framework was proposed by incorporating merits of the GSQH and the histogram-based embedding. In comparison with the existing LDE methods, the proposed one has better utilized the statistical characteristics of images and achieved better adaptability, flexible capacity control, and higher security. Thorough experimental studies show that this framework performs better than the conventional LDE methods based on the GH, and the method simply using the AADH. There are several directions for future work including the development of new image statistical characteristics to construct a more efficient embedding carrier. In addition, we planned to enhance the robustness of the proposed framework based on the successful experiences of other techniques [8], [16], [17], [23], e.g, clustering [26], [27], human visual system [15], [22], feature point [6], [7], [13], [14].

Acknowledgment

The authors would like to thank the anonymous reviewers for their helpful comments and suggestions.

References

[1] L. An, X. Gao, C. Deng, and F. Ji, "Reversible watermarking based on statistical quantity histogram," in *Proc. Adv. Multimedia Inform. Process.*, LNCS 5879. 2009, pp. 1300–1305.
[2] L. An, X. Gao, C. Deng, and F. Ji, "Robust lossless data hiding: Analysis and evaluation," in *Proc. Int. Conf. High Performance Comput. Simul.*, 2010, pp. 512–516.

[3] L. An, X. Gao, and C. Deng, "Reliable embedding for robust reversible watermarking," in *Proc. ACM Int. Conf. Internet Multimedia Comput. Service*, 2010, pp. 57–60.
[4] J. Barton, "Method and apparatus for embedding authentication information within digital data," U.S. Patent 5 646 997, Jul. 8, 1997.
[5] C. Vleeschouwer, J. Delaigle, and B. Macq, "Circular interpretation of bijective transformations in lossless watermarking for media asset management," *IEEE Trans. Multimedia*, vol. 5, no. 1, pp. 97–105, Mar. 2003.
[6] C. Deng, X. Gao, X. Li, and D. Tao, "A local Tchebichef moments-based robust image watermarking," *Signal Process.*, vol. 89, no. 8, pp. 1531–1539, Aug. 2009.
[7] C. Deng, X. Gao, X. Li, and D. Tao, "Local histogram based geometric invariant image watermarking," *Signal Process.*, vol. 90, no. 12, pp. 3256–3264, Dec. 2010.
[8] C. Deng, X. Gao, H. Peng, L. An, and F. Ji, "Histogram modification based robust image watermarking approach," *Int. J. Multimedia Intell. Security*, vol. 1, no. 2, pp. 153–168, 2010.
[9] M. Fallahpour, "Reversible image data hiding based on gradient adjusted prediction," *IEICE Electron. Exp.*, vol. 5, no. 20, pp. 870–876, Oct. 2008.
[10] J. Fridrich, M. Goljan, and R. Du, "Lossless data embedding: New paradigm in digital watermarking," *EURASIP J. Appl. Signal Process.*, vol. 2002, no. 2, pp. 185–196, Jan. 2002.
[11] J. Fridrich, M. Goljan, and R. Du, "Invertible authentication," *Proc. SPIE Security Watermarking Multimedia Contents III*, vol. 4314, pp. 197–208, Jan. 2001.
[12] X. Gao, L. An, X. Li, and D. Tao, "Reversibility improved lossless data hiding," *Signal Process.*, vol. 89, no. 10, pp. 2053–2065, Oct. 2009.
[13] X. Gao, C. Deng, X. Li, and D. Tao, "Geometric distortion insensitive image watermarking in affine covariant regions," *IEEE Trans. Syst. Man Cybern. C Appl. Rev.*, vol. 40, no. 3, pp. 278–286, May 2010.
[14] X. Gao, C. Deng, X. Li, and D. Tao, "Local feature based geometric-resistant image information hiding," *Cogn. Comput.*, vol. 2, no. 2, pp. 68–77, Mar. 2010.
[15] X. Gao, W. Lu, D. Tao, and X. Li, "Image quality assessment based on multiscale geometric analysis," *IEEE Trans. Image Process.*, vol. 18, no. 7, pp. 1409–1423, Jul. 2009.
[16] X. Gao, Y. Wang, X. Li, and D. Tao, "On combining morphological component analysis and concentric morphology model for mammographic mass detection," *IEEE Trans. Inf. Technol. Biomed.*, vol. 14, no. 2, pp. 266–273, Mar. 2010.
[17] X. Gao, B. Wang, D. Tao, and X. Li, "A relay level set method for automatic image segmentation," *IEEE Trans. Syst. Man Cybern. B Cybern.*, vol. 41, no. 2, pp. 518–525, Apr. 2011.
[18] C. Honsinger, P. Jones, M. Rabbani, and J. Stoffel, "Lossless recovery of an original image containing embedded data," U.S. Patent 6 278 791 B1, Aug. 21, 2001.
[19] J. Hwang, J. Kim, and J. Choi, "A reversible watermarking based on histogram shifting," in *Proc. Digit. Watermarking*, LNCS 4283. 2006, pp. 348–361.
[20] Z. Ni, Y. Shi, N. Ansari, W. Su, Q. Sun, and X. Lin, "Robust lossless image data hiding designed for semi-fragile image authentication," *IEEE Trans. Circuits Syst. Video Technol.*, vol. 18, no. 4, pp. 497–509, Apr. 2008.
[21] Z. Ni, Y. Shi, N. Ansari, and W. Su, "Reversible data hiding," *IEEE Trans. Circuits Syst. Video Technol.*, vol. 16, no. 3, pp. 354–362, Mar. 2006.
[22] D. Song and D. Tao, "Biologically inspired feature manifold for scene classification," *IEEE Trans. Image Process.*, vol. 19, no. 1, pp. 174–184, Jan. 2010.
[23] M. Song, D. Tao, C. Chen, X. Li, and C. Chen, "Color to gray: Visual cure preservation," *IEEE Trans. Pattern Anal. Mach. Intell.*, vol. 32, no. 9, pp. 1537–1552, Sep. 2010.
[24] W. Tai, C. Yeh, and C. Chang, "Reversible data hiding based on histogram modification of pixel differences," *IEEE Trans. Circuits Syst. Video Technol.*, vol. 19, no. 6, pp. 906–910, Jun. 2009.
[25] J. Tian, "Reversible watermarking using a difference expansion," *IEEE Trans. Circuits Syst. Video Technol.*, vol. 13, no. 8, pp. 890–896, Aug. 2003.
[26] T. Xia, D. Tao, T. Mei, and Y. Zhang, "Multiview spectral embedding," *IEEE Trans. Syst. Man Cybern. B Cybern.*, vol. 40, no. 6, pp. 1438–1446, Dec. 2010.
[27] T. Zhou and D. Tao, "Fast gradient clustering," in *Proc. NIPS Workshop Discr. Optim. Mach. Learn.: Submodularity Sparsity Polyhedra*, 2009, pp. 1–6.
[28] *CVG-UGR Image Database* [Online]. Available: http://decsai.ugr.es/cvg/dbimagenes/index.php
[29] *Brodatz Textures* [Online]. Available: http://www.ux.uis.no/~tranden/brodatz.html
[30] *DICOM Sample Image Sets* [Online]. Available: http://pubimage.hcu-ge.ch:8080
[31] *OsiriX* [Online]. Available: http://www.osirix-viewer.com/Downloads.html

Xinbo Gao (M'02–SM'07) received the B.S., M.S., and Ph.D. degrees in signal and information processing from Xidian University, Xi'an, Shaanxi, China, in 1994, 1997, and 1999, respectively.

From 1997 to 1998, he was a Research Fellow with the Department of Computer Science, Shizuoka University, Shizuoka, Japan. From 2000 to 2001, he was a Post-Doctoral Research Fellow with the Department of Information Engineering, Chinese University of Hong Kong, Shatin, Hong Kong. Since 2001, he has been with the School of Electronic Engineering, Xidian University. Currently, he is a Professor of pattern recognition and intelligent systems and the Director of the VIPS Laboratory, Xidian University. His current research interests include computational intelligence, machine learning, computer vision, pattern recognition, and wireless communications. In these areas, he has published 4 books and around 100 technical articles in refereed journals and proceedings, including IEEE TRANSACTIONS ON IMAGE PROCESSING, IEEE TRANSACTIONS ON CIRCUITS AND SYSTEMS FOR VIDEO TECHNOLOGY, IEEE TRANSACTIONS ON NEURAL NETWORKS, IEEE TRANSACTIONS ON SYSTEMS, MAN AND CYBERNETICS, *Pattern Recognition*, and so on.

Dr. Gao is on the editorial boards of several journals, including *EURASIP Signal Processing (Elsevier)* and *Neurocomputing (Elsevier)*. He served as the general chair/co-chair or program committee chair/co-chair or a PC member for around 30 major international conferences.

Lingling An received the B.S. and M.S. degrees in computer science and technology from Xidian University, Xi'an, Shaanxi, China, in 2002 and 2005, respectively. She is currently pursuing the Ph.D. degree in intelligent information processing from the School of Electronic Engineering, Xidian University.

Her current research interests include lossless data hiding, digital watermarking, and machine learning.

Yuan Yuan (M'05–SM'09) is currently a Researcher (Full Professor) with the Center for OPTical IMagery Analysis and Learning (OPTIMAL), State Key Laboratory of Transient Optics and Photonics, Xi'an Institute of Optics and Precision Mechanics, Chinese Academy of Sciences, Xi'an, Shaanxi, China.

Dacheng Tao (M'07) received the B.Eng. degree from the University of Science and Technology of China, Hefei, Anhui, China, the M.Phil. degree from the Chinese University of Hong Kong, Shatin, Hong Kong, and the Ph.D. degree from the University of London, London, U.K.

Currently, he is a Professor with the Center for Quantum Computation and Information Systems and the Faculty of Engineering and Information Technology, University of Technology, Sydney, Australia. He mainly applies statistics and mathematics for data analysis problems in data mining, computer vision, machine learning, multimedia, and video surveillance. He has authored and co-authored more than 100 scientific articles at top venues including IEEE T-PAMI, T-KDE, T-IP, NIPS, AISTATS, AAAI, CVPR, ECCV, ICDM, ACM T-KDD, and KDD.

Dr. Tao has earned several best paper awards for his contributions. He serves as an Associate Editor of the IEEE TRANSACTIONS ON KNOWLEDGE AND DATA ENGINEERING and the *Official Journal of the International Association for Statistical Computing—Computational Statistics and Data Analysis (Elsevier)*.

Xuelong Li (M'02–SM'07) is currently a Researcher (Full Professor) with the Center for OPTical IMagery Analysis and Learning (OPTIMAL), State Key Laboratory of Transient Optics and Photonics, Xi'an Institute of Optics and Precision Mechanics, Chinese Academy of Sciences, Xi'an, Shaanxi, China.